IEEE Photonics Journal
An IEEE Photonics Society Publication

Open Access

Enhancement of the Au/ZnO-NA Plasmonic SERS Signal Using Principal Component Analysis as a Machine Learning Approach

Volume 12, Number 5, October 2020

Akhilesh Kumar Gupta, *Student Member, IEEE*
Chih-Hsien Hsu
Chao-Sung Lai, *Senior Member, IEEE*

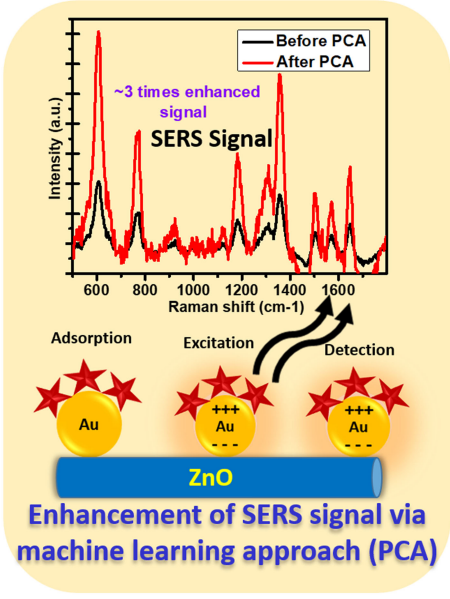

DOI: 10.1109/JPHOT.2020.3015740

IEEE photonics SOCIETY
IEEE

Enhancement of the Au/ZnO-NA Plasmonic SERS Signal Using Principal Component Analysis as a Machine Learning Approach

Akhilesh Kumar Gupta,[1] ***Student Member, IEEE*****, Chih-Hsien Hsu,**[1] **and Chao-Sung Lai** ,[1,2,3,4,5] ***Senior Member, IEEE***

[1]Department of Electronic Engineering, Chang Gung University, Taoyuan, Taiwan
[2]Department of Nephrology, Chang Gung Memorial Hospital, Taoyuan, Taiwan
[3]Department of Materials Engineering, Ming-Chi University of Technology, New Taipei City, Taiwan
[4]Artificial Intelligent Research Center, Chang Gung University, Taoyuan, Taiwan
[5]Biomedical Research Center, Chang Gung University, Taoyuan, Taiwan

DOI:10.1109/JPHOT.2020.3015740

Manuscript received June 29, 2020; accepted August 7, 2020. Date of publication August 11, 2020; date of current version September 3, 2020. This work was supported in part by the Ministry of Science and Technology, Taiwan under Project MOST 109-2221-E-182-013-MY3 and MOST 108-2218-E-182-002, and in part by Chang Gung Memorial Hospital Research Project under Grants CMRPD2K0051 and CORPD2J0071. Corresponding author: Chao-Sung Lai (e-mail: cslai@mail.cgu.edu.tw).

Abstract: In this work, we modeled a novel approach to enhance surface-enhanced Raman scattering (SERS) signals using principal component analysis (PCA) as a machine learning approach. Zinc oxide nanoarrays (ZnO-NAs) were synthesized using a hydrothermal method followed by zinc oxide nucleation on ITO glass substrates via an oxidation furnace at 500 °C. The surface morphology was improved by short rapid thermal annealing (S-RTA) after deposition of a gold layer via a thermal evaporator to avoid chemical contamination of the sensing surface, which is a suitable plasmonic platform for the generation of "hot spots" for SERS enhancement with fewer defects. The proposed Au/ZnO-NA SERS sensor exhibited an enhancement factor (EF) of 1.15×10^7 via the R6G Raman probe and excellent uniformity over the entire surface. The PCA algorithm was used to extract useful features and information from the SERS signal. The algorithm was implemented with MATLAB software (R2019a) by the multivariable analytical tool to find an enhanced signal ($\sim$3 times higher) with high uniformity, which has great potential and is applicable to a wide range of probe molecules suitable in medical, safety, and environmental applications.

Index Terms: Plasmonic model, SERS, signal enhancement, PCA analysis, machine learning approach.

1. Introduction

In sensing applications, signal amplification and the signal-to-noise ratio play a critical role. Strong electric field confinement and scattering phenomena due to contact of a metallic object with a nanoscale object lead to plasmonic effects that result in an electric field called surface-enhanced Raman scattering (SERS) [1]. Although the SERS technique has been extensively studied over the past ten years due to a drastic advancement in nanotechnology, the implementation of highly sensitive and stable SERS as simple analytical tools remains a major challenge [2], [3].

The enhancement factor (EF) is known to be a SERS criterion for the ability to differentiate between low energy levels and the sensitivity of the SERS surface. A high EF value of 10^8 is known to be adequate to detect a single molecule [4]. The electromagnetic (EM) effect is based on the enhancement of the EM field due to localized conduction electron and oscillation resonance excitations at the surface of metal nanostructures. The EM enhancement depends on metal characteristics and molecular distance from the surface. Researchers have tried to improve SERS as well as the plasmonic behavior by testing the shape and size of plasmonic nanoparticles such as silver (AgNPs) and gold nanoparticles (AuNPs) [5], [6]. In comparison to other thicker structures of AuNPs, our group has researched different sizes of NPs and the tunable plasmonic behavior of ZnO-NR [7]. Moreover, weak SERS signals may not provide enough information to clearly identify specific diseases. Numerous methods, including principal component analysis (PCA) and independent component analysis (ICA), can be used [8]. These methods are well-established methods for reducing the dimensionality, and are commonly used for avoiding redundancy due to high-dimensional data [9]. Thus, PCA as a machine learning approach was used to compute multivariate statistics to identify specific diseases with a strong enhanced signal. Additionally, researchers have published a label-free biological classification system based on an Au/ZnO-NR/G sensor that was implemented using a PCA projected SVM-classified calculation algorithm. The group used aqueous human tumor samples from patients with cataracts and two oxidative stress-induced eye diseases, which were analyzed using the proposed sensor [10]. Researchers have demonstrated a SERS platform to help ensure normal delivery without infection and premature delivery of maternal diseases. Their SERS platform could detect the presence and identification of prenatal diseases with the assistance of a machine learning approach using the PCA-SVM for amniotic fluids with high sensitivity [11]. In addition, studies have examined the application of Raman spectroscopy to oral cryopreserved tissues with fresh excisions and the potential to increase the efficiency of oral cancer screening procedures to recognize a tumor-free margin of resection during surgery by PCA-QDA [12].

Zinc oxide (ZnO) is a well-known working material with suitable morphologies that can be optimized by a simple and cost-efficient manufacturing process. ZnO, as a semiconductor, is promising and biocompatible with a small direct bandgap (~3.4 eV) [13]. Moreover, ZnO is synthesized naturally with defects due to the impurity of the crystal structure. Therefore, the synthesized ZnO needs to be engineered to minimize the defects to increase the charge separation process upon light absorption [14]. Vacancies of interstitial oxygen and zinc are two commonly intrinsic defects reported to be beneficial for potential photocatalysis. The defects were noted to contribute to the formation of $O_2{}^{-2}$ on the ZnO-NR surface by trapping electrons and holes with adsorbed oxygen and hydroxyl groups [15]. Furthermore, the interaction of strong SERS operation when ZnO is combined with plasmonic metals can be assured not only by the surface plasmons but also by the interactions of charge-transfer (CT) between semiconductors and metals in several applications [16].

In this work, gold was deposited via a thermal evaporator after the synthesis of ZnO-NAs using a hydrothermal process. After the production of Au/ZnO-NA substrates, a short rapid thermal annealing (S-RTA) process on the substrate was conducted at 650 °C to increase the surface roughness, which contributes to the SERS activity. Later, we modeled the PCA algorithm as a machine learning approach for an enhanced signal with high intensity. These methods are expected to expand to different research areas in the future, as they apply to other types of spectroscopies and the spectroscopic field of deep learning and artificial intelligence data processing, and can be used for the extraction of sufficient information to identify specific diseases.

2. Experimental Details

Fabrication of the Au/ZnO-NA platform and explanation of SERS activity are shown in Fig. 1. ZnO-NAs were grown on ITO with a glass substrate size of 2 × 2 cm^2. The ITO/glass substrates were washed with deionized water, acetone, and alcohol and dried with N_2 flow. The precursor solution was prepared by dissolving 5 mM zinc acetate $Zn(CH_3COO)_2{\bullet}2H_2O$ in pure ethanol. The ZnO

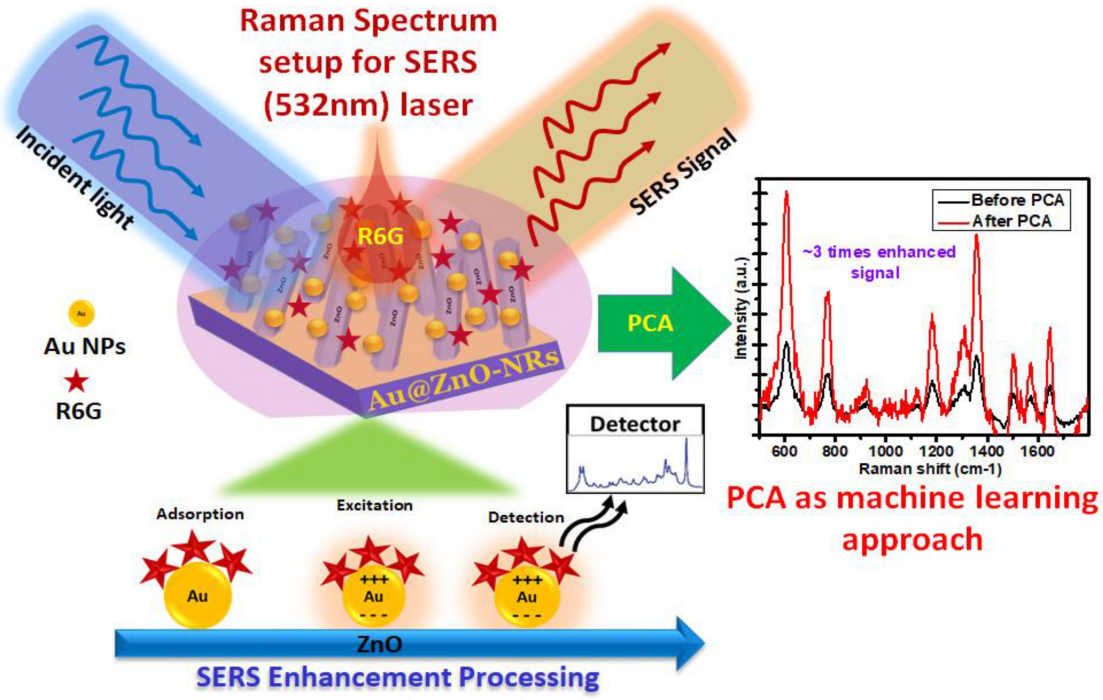

Fig. 1. Schematic diagram of the proposed plasmonic SERS model and enhancement process.

precursor solution was deposited onto the ITO-coated glass substrate by the dip-coating process. To create a ZnO seed layer on ITO, the as-deposited film substrates were annealed in air at 500 °C for 30 min. The step-by-step process started from seeding layers and growth of ZnO-NAs using the hydrothermal method [7].

2.1 Plasmonic Substrate

After ZnO-NA growth on ITO as described above, a gold layer thickness of 3 nm was deposited on top of the ZnO-NA layer via a thermal evaporator. The evaporation method was performed to avoid chemical contamination and reactions with the sensing surface. To generate hot spots due to the plasmonic nature of the substrate, S-RTA (650 °C) was used after the deposition of gold (3 nm) on ZnO-NAs for the detection of R6G (10^{-4} M). S-RTA (650 °C) treatment of the noble metal on ZnO-NAs is one of the most frequently used methods to narrow the gap within coalesced nanoparticles to generate hot spots due to plasmon coupling [17]. Moreover, S-RTA treatment substantially changed the curve shape, absorption intensity, and position of $\lambda_{\max}$ of the LSPR signal due to the thickness and interstitial distance of aggregated gold nanoparticles created by S-RTA treatment [18].

2.2 Surface Morphology, Roughness, and SERS Analysis

Surface images were obtained by transmission electron microscopy (TEM, JEOL, JEM-ARM200FTH, Japan), while the roughness of the surface was analyzed by AFM performed in tapping mode with a scanning region of 1×1 μm^2 (Innova B067, Bruker Corp. USA). For SERS analysis, 10^{-4} M R6G molecules were dropped onto the substrate, and SERS detection was performed by a Raman System using a 532 nm excitation wavelength. The excitation and light processing were achieved using a 100 x objective lens (NA 0.5) with a laser power of 50 mW

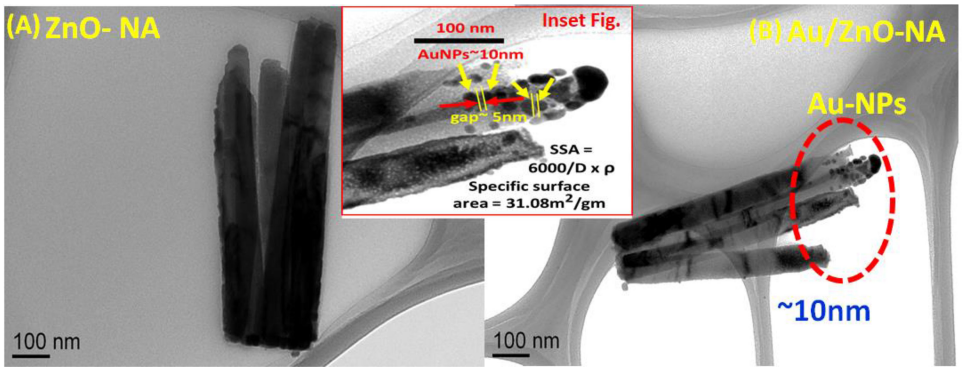

Fig. 2. TEM images of (A) ZnO nanoarrays after S-RTA treatment and (B) the interface of ZnO nanoarray and Au nanoparticles; (inset) AuNPs with nanogaps and calculated specific surface area.

and an exposure time of 2 seconds with 3 accumulations. The SERS signals were collected and assessed by baseline extraction of ten different spots. To analyze the TEM sample, ZnO-NAs and Au/ZnO-NAs were dispersed in ethanol by ultrasonic agitation and the suspension was dropped on lacey carbon-coated grids.

2.3 Multivariate Analysis (PCA) as Machine Learning

Principal component analysis (PCA) is the most popular multifunction statistical method as a machine learning approach and is used in almost every scientific discipline [19]. The objectives of PCA are collecting the most important data from a big data set. It compresses the data to collect only useful information, simplify the data set, and evaluate the observation structure and variables [20].

For a data matrix with p variables and n samples, the data are based on each variable and mean first. This approach ensures that the data cloud concentrates on the origin and the spatial reference of the data or the variances of the variables. A linear combination of the variables X_1, X_2 ... X_P is used to describe the first principal components (Y_1).

$$Y_1 = a_{11}x_1 + a_{12}x_2 + \cdots\cdots\cdots + a_{1p}x_p \tag{1}$$

In calculating the first principal variable, the maximum variability from the data set is considered. The other principal component is measured in the same way but is not associated with the next maximum variance with the first principal component.

$$Y_2 = a_{21}x_1 + a_{22}x_2 + \cdots\cdots\cdots + a_{2p}x_p \tag{2}$$

The calculations are carried out until a total of p major components equal to the original number of variables are determined. The sum of the variances from all principal components is now equal to the sum of the variables, i.e., the original information has been clarified [21].

3. Results

TEM and AFM were conducted to investigate the structure and morphology of the ZnO nanoarrays and the gold-coated ZnO-NAs. The formation of ZnO-NAs and Au nanoparticles (NPs) on the surface of the ZnO nanoarrays is depicted from the micrographs in Fig. 2. The length of ZnO-NAs was 1 μm, the diameter of nanoarrays was 100$\sim$120 nm and the diameter of the AuNPs coated onto ZnO-NA was approximately 10 nm. Fig. 2 (B) revealed the formation of AuNPs supported by long ZnO nanoarrays due to the S-RTA effect [22]. The detailed morphology and surface roughness of the Au-deposited ZnO were examined by AFM. Fig. 3 shows the AFM 3D images, which

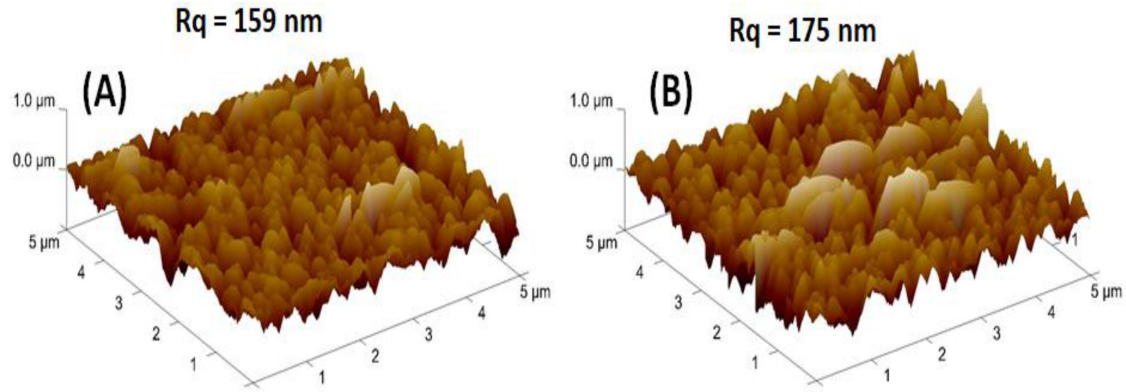

Fig. 3. The surface roughness of the ZnO-NA substrate and ZnO-NA substrate coated with 3 nm thick Au.

indicate the vertical c-axis-oriented growth of the nanoarrays and confirm the typical observations for wurtzite ZnO with Rq and Ra values of 159 and 124 nm, respectively. An increase in the RMS surface roughness values of 175 and 137 were observed upon Au (3 nm) deposition due to the increase in the grain size. The increase in the surface roughness of the substrate was associated with a large volume-to-size ratio. Compared with Au/ZnO-NAs, Au substrates showed higher surface roughness than ZnO grown on bare ITO [23]. Fig. 1 defines the underlying localized surface plasmon resonance (LSPR) improvement mechanism for SERS on the Au/ZnO substrate. The gold nanoparticle surface coverage should be high to maximize the immobilization of R6G molecules onto the gold nanoisland areas of the Au/ZnO-NA substrate. To generate hot spots due to the plasmonic nature of the substrate, S-RTA (650 °C) was used after the deposition of gold (3 nm) on ZnO-NAs for the detection of R6G. S-RTA treatment of the noble metal on ZnO-NAs is one of the most frequently used methods to narrow the nanoparticle band gap and generate hot spots. Hot spots are generated by isolated groups of gold nanoparticles that self-assemble on the ZnO surface. From Fig. 2, TEM (inset) shows ∼10 nm AuNPs with ∼5 nm nanogaps between two NPs, a hot gap from which we can expect a great value of Raman intensity. The values of EF are very sensitive to the morphology of the deposited AuNPs on ZnO due to the contribution of active hot spot regions and the absence of ineffective large-sized nanoparticle regions. The shape of nanoparticles is related to EF, and EF can be increased by increasing the nanoparticle specific surface area [24]. Increasing the nanoparticle surface area could significantly boost the Raman signal. The boost is achieved because nanoparticles are highly exposed and energy transfers within the hot spot regions are effective. The specific surface area is given as [25],

$$\text{Specific surface area} = 6000/\text{Dx}\rho = 31.08\ \text{m}^2/\text{gm}$$

Where D is the size of the AuNPs and ρ is the density of gold (19.3 g/cm^3). Here, we used 6000 as form factor values for isothermal particles. In general, the known SERS effect caused by the charge transfer (CT) effect can be explained by the fact that an incident photon excites an electron from the metal surface into an adsorbed molecule, creating a negatively charged excited molecule. CT induces nuclear relaxation of the excited molecule, leading to the return of the electron to the metal surface and the formation of an exciting neutral molecule with the emission of a shifted wavelength. This results in a similar “donor–bridge–acceptor” CT mode, which occurs more easily in the AuNPs/ZnO/molecule system due to the principle of energy level. The transfer of the direct charge between Au and R6G is not possible because of the large energy difference. We used an excitation laser of 532 nm (2.33 EV) with work functions of gold (5.1), ZnO (5.3), and R6G (2.3). Metal and semiconductor junctions, as Schottky barriers between Au and ZnO-NAs, are related to the (charge transfer) CT mechanism via the SERS model shown in Fig. 4(A) [26], [27]. Furthermore,

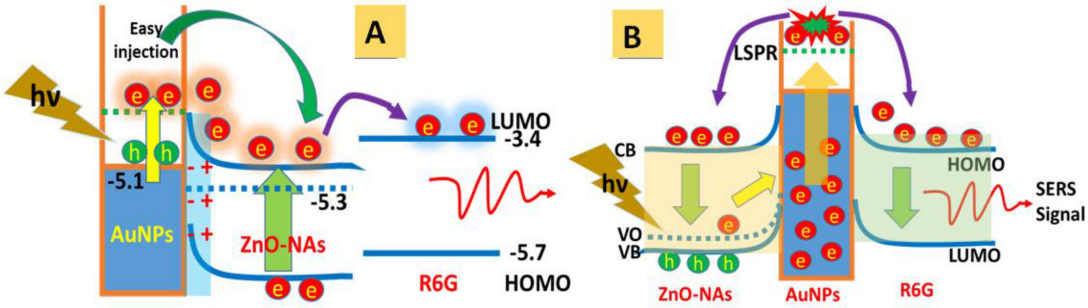

Fig. 4. (A) R6G/AuNPs/ZnO-NAs assisted charge transfer (CT) SERS model; (B) Mechanism of the enhanced signal via LSPR energy levels.

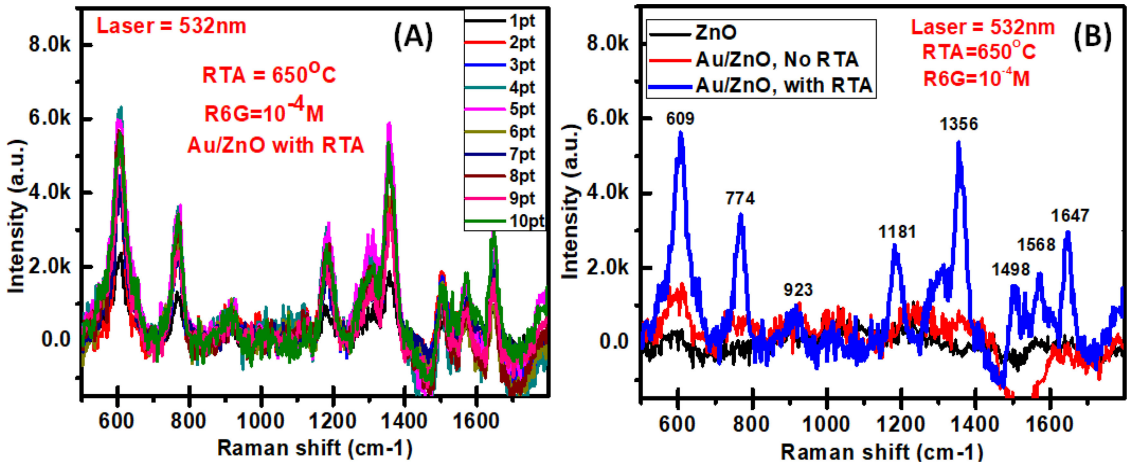

Fig. 5. (A) Spots of 10 SERS spectra of R6G over AuNPs/ZnO-NA; (B) detection of the R6G analyte with a control sample.

R6G peaks were verified by SERS spectra, and detection of the chemical band of the molecule is shown in Fig. 5(A and B) [28].

The localized surface plasmon resonance (LSPR) energy level is enhanced due to the strong electron transition to a higher level. The defect in ZnO is strongly linked to the vacancy of oxygen (VO) and the resulting narrow bandgap via the engineered structure [29]. Thus, the VO forms an energy level slightly above the valence band of ZnO. Due to the seeding temperature and S-RTA treatment, the defects in the structure play an important role in the electron transition between energy levels. The occurrence of defects in ZnO-NAs substantially affects the energy transition of the AuNPs coated on ZnO-NAs due to differences in the amount of electron excitation at the LSPR energy level of the AuNPs. During the electron transition from the ZnO conduction band (CB) to the valence band (VB), electrons are trapped in the VO level, and some electrons migrate directly to the Au region. Defects and the resulting narrow bandgap in ZnO result in a high number of electrons in the VO level, which reduces the energy transfer to the AuNPs, while a defectless surface reduces the number of trapped electrons in the VO level and allows a strong energy transition to the AuNPs. However, the crucial role of the electron transition, in which fast electrons transfer to higher energy levels is generally improved by the LSPR energy level details, is shown in Fig. 4(B). Moreover, in the LSPR energy state, the amount of electron excitation also affects R6G injection and increases the signal intensity. Increased electron injection in the LSPR energy state results in an increase in the signal of R6G [7]. In addition, for a free-metal electron,

TABLE 1
Comparison Table of the Existing SERS Method and Detection of Disease via a Machine Learning Approach

Substrate	Experimental method	Detection	Enhancement factor	Techniques	Ref.
Au/ZnONR/G (SERS)	Sputter/ Hydrothermal	R6G, aqueous humor, eye disease	2.3×10^6	PCA-SVM	[10]
Au/ZnO Nanorods (SERS)	Sputter/ Hydrothermal	IC/BPS animal urinary, Bladder Pain Syndrome	Not mentioned	PCA	[32]
AuNPs liquid (SERS)	Chemical process	blood serum, Colorectal Cancer	Not mentioned	PCA-SVM	[33]
AuNPs/ZnO-NAs (Plasmonic SERS)	**Thermal evap./ Hydrothermal (Avoid chemical contamination)**	**R6G (Rhodamine)**	**$1.15X10^7$**	**PCA (Machine learning)**	**Present work**

according to the momentum of conservation, the direction of generated hot electrons should mainly be along the oscillation direction of LSPR. However, the oscillation of LSPR along the interface of the metal-semiconductor composite generates hot electrons that move to the semiconductor and thus increase the hot electron generation efficiency (HEGE) [30]. SERS measurements were conducted on R6G on AuNPs/ZnO-NAs, averaged from SERS spectra taken at 10 spots, as shown in Fig. 5(A), and R6G (10^{-4} M) was detected and compared with a control sample, as shown in Fig. 5(B).

The SERS enhancement factor (EF-SERS) is calculated based on the following equation [17], [31]:

$$EF_{\text{SERS}} = \frac{I_{\text{SERS}}/N_{\text{SERS}}}{I_{R6G(\text{bare})}/N_{R6G(\text{bare})}} \tag{3}$$

where I_{SERS} and I_{bare} are the Raman intensities of the molecule on the SERS surface and on the bare substrate, respectively, and N_{SERS} and N_{bare} are the numbers of adsorbed molecules in the scattering volume on the SERS and non-SERS substrates. N_{SERS} can be calculated by using the surface density of R6G and the area of the laser spot as 39.87×10^{-16} moles. For the N_{bare} sample, the sampling volume is the product of the area of the laser spot and penetration of the laser beam. Taking the density of bulk R6G into account, N_{bare} can be calculated to be 160×10^{-10} moles. Finally, the SERS EF is determined to be 1.15×10^7 for the R6G peak at 1356 cm^{-1}. To produce an effective enhanced SERS signal, PCA is used as a machine learning approach that plays an important role in collecting useful information from the data set and provides improved extraction of the desired (3 times higher) signal.

3.1 PCA Techniques for the Analysis of Raman Spectra

The theories and methodologies for signal processing by the PCA technique are discussed in this section. The signal processing techniques used in Raman spectra for disease detection in our literature review are summarized in Table 1. PCA is a multivariate evaluation technique to minimize dimension and/or classification without supervision. By decreasing redundancy and noise, it transforms a massive amount of data into fewer new variants. The structure and vicinity

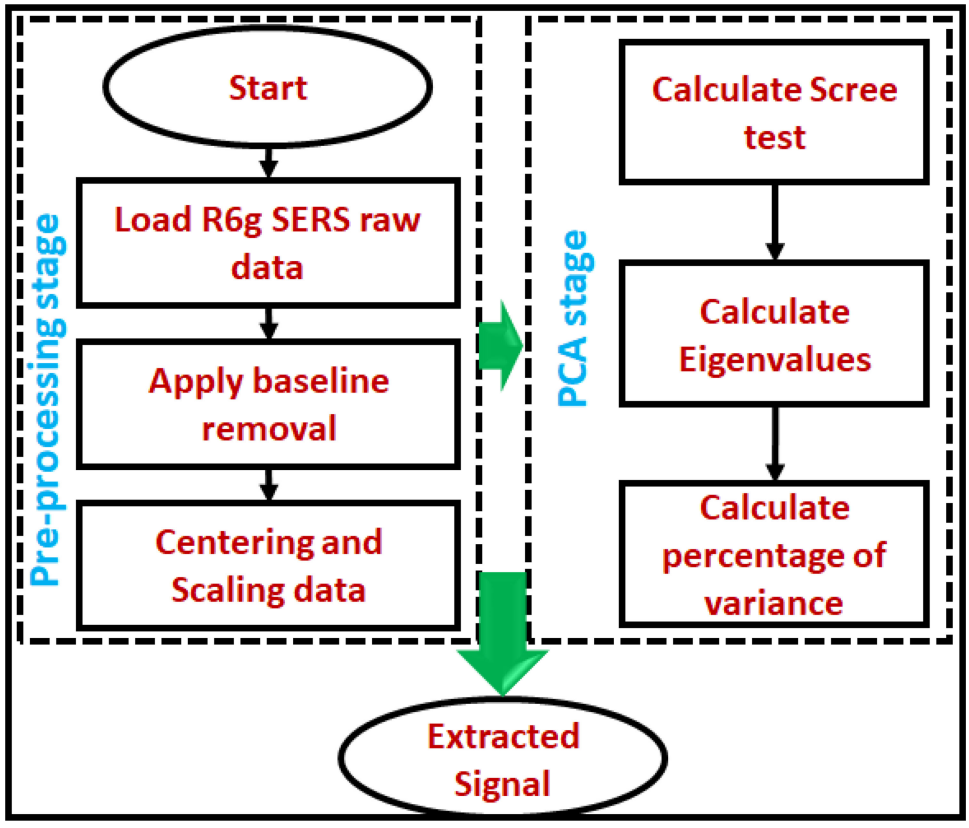

Fig. 6. Flowchart for the principal component analysis model.

of the original spectrum change after the transition of the spectrum to another space. This makes it useful for the analysis of Raman spectra obtained from biological samples, which contain a high volume of data with complex characteristics. PCA reduces the usually high volume of spectral data to a few principal components and a combination of new data sets given by equation (1 & 2). Here, Fig. 6 describes the steps flow chart towards the development of the PCA algorithm. The SERS spectra were collected from 10 sequential spots on the same sample, with a 10-second accumulation collected at each spot (438 observations and 10 variable data). First, PCA transforms the input feature data into an orthogonal space using an orthogonal linear transformation, which is illustrated in Fig. 7(A). The outcome is orthogonal components known as PCs, and second, the PCs are arranged according to their variance. Variance is a sample distribution function of variability, which is expressed as the average square deviation of each sample from its mean [19], [20],

$$\text{Variance} = \frac{\Sigma(\text{Sample}_{\text{SERS}} - \text{mean})^2}{\text{total\_sample}} \tag{4}$$

While the percentage of variance is given as follows.

$$\%\,\text{of variance} = \frac{100 \times \text{Variance}(n^{\text{th}}\text{PC}_S)}{\text{total\_variance}} \tag{5}$$

The last step eliminates PCs with the least input to the data set variance. A selection of PCs is adequate in practice for the overall variability of the observed variables. The more variant PCs are counted first, while the less variant PCs are ranked last. However, in practice, the cost function is

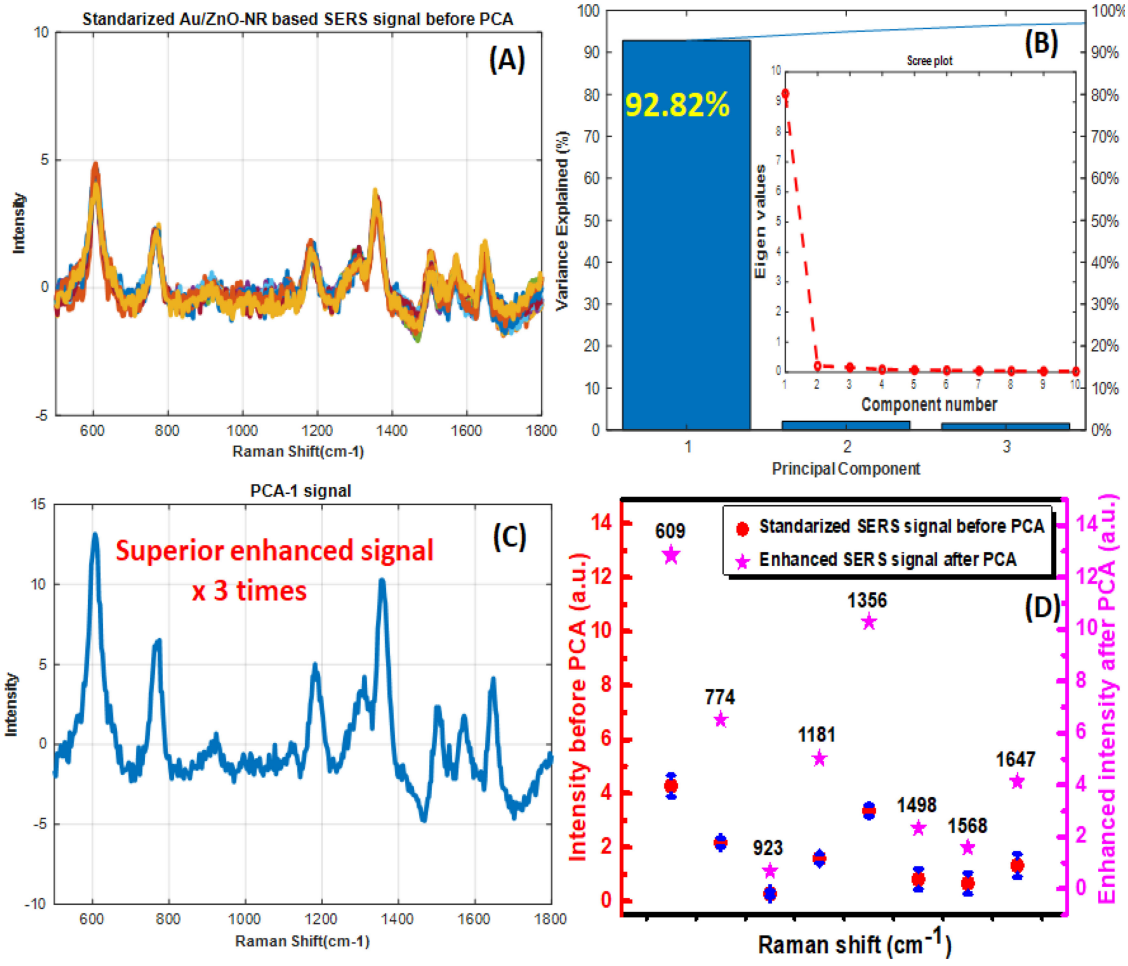

Fig. 7. (A) Standardized AuNPs/ZnO-NA SERS signal before PCA. (B) The scree plot shows the first two (instead of the total 10) components that explain 95% of the total variance. (C) Enhanced SERS signal after PCA. (D) Comparison of an enhanced signal before and after the PCA model.

used in addition to ranking the significance of PC components: (1) Eigenvalue: This criterion keeps PCs with an eigenvalue equal to or greater than one, as shown in Fig. 7(B), because their variance is higher, and (2) scree test: This is usually used in conjunction with the eigenvalue and plots the graphic representation of the relationship between eigenvalues and PCs as illustrated in Fig. 7(B, inset). The scree plot only shows the first three (instead of the total 10) components that explain 96.50% of the total variance. The only clear difference is the amount of variance shown between the first, second, and third components; the remaining components with small variances are eliminated. The intensity of the SERS signal before and after PCA from AuNPs/ZnO-NAs with R6G at the Raman shift peak is plotted in Fig. 7(D). This indicates that at high seeding temperature [34], the ZnO-NAs produced fewer defects on their surface and showed more effective enhancement of the R6G SERS signal. Moreover, after PCA, the signal is much larger (~3 times higher) than the signal before PCA. Thus, the first 3 components explain 96.50% of the variation. For the subsequent analysis, we can only keep those 3 dimensions (first 3 columns of PCs) and 438 observations instead of 10 variables. From the above discussion and results, we conclude that PCA as a machine learning tool can provide sufficient information on weak signals and can identify specific disease information in future studies.

4. Conclusion

We established a highly sensitive and practical method with an AuNP/ZnO-NA SERS sensor platform merged with multivariate statistics as a machine learning tool for the detection of R6G molecules with an enhanced (3 times higher) signal. The AuNP/ZnO-NA SERS platform was designed via two different procedures: a low-cost solution-processed ZnO seed layer and the hydrothermal growth of ZnO-NAs on an ITO glass plate for nanostructure fabrication after thermal evaporator-induced gold NPs on the ZnO-NAs. Further S-RTA treatment was applied to the gold-coated ZnO for synergetic enhancement of the plasmonic activity. In addition to the efficiency of commercial SERS substrates, our AuNPs/ZnO-NA SERS sensors achieved an EF of 1.15×10^7 with excellent uniformity. To promote the practical applicability of our SERS platform, multivariate statistics-derived machine learning tools were applied to the AuNP/ZnO-NA platform. This method is expected to expand to other areas of research in the near future since it applies to other types of spectroscopies as well as the spectroscopic field of deep learning and artificial intelligence data processing, and it can be used for the extraction of sufficient information to identify specific diseases.

References

[1] G. Barbillon *et al.*, "Study of Au coated ZnO nanoarrays for surface enhanced Raman scattering chemical sensing," *J. Mater. Chem. C*, vol. 5, no. 14, pp. 3528–3535, 2017.

[2] Y. Li, L. Zhou, L. Tang, M. Li, and J. J. He, "Improved surface enhanced Raman scattering based on hybrid Au nanostructures for biomolecule detection," *IEEE Photon. J.*, vol. 8, no. 6, 2016 Art. no. 6806007.

[3] G. Youfu, Y. Zhen, T. Xiaoling, D. Yu, H. Xueming, and L. Xuejin, "Femtosecond laser ablated polymer SERS fiber probe with photoreduced deposition of silver nanoparticles," *IEEE Photon. J.*, vol. 8, no. 5, 2016 Art. no. 4502006.

[4] D. Radziuk and H. Moehwald, "Prospects for plasmonic hot spots in single molecule SERS towards the chemical imaging of live cells," *Phys. Chem. Chem. Phys.*, vol. 17, no. 33, pp. 21072–21093, 2015.

[5] P. Guo *et al.*, "Plasmonic core-shell nanoparticles for SERS detection of the pesticide thiram: Size- and shape-dependent Raman enhancement," *Nanoscale*, vol. 7, no. 7, pp. 2862–2868, 2015.

[6] T. Dixit *et al.*, "Plasmon-assisted selective enhancement of direct-band transitions in multi-layer MoS 2," *IEEE Photon. J.*, vol. 11, no. 5, 2019 Art. no. 4501106.

[7] A. K. Gupta *et al.*, "Au-spotted zinc oxide nano-hexagonrods structure for plasmon-photoluminescence sensor," *Sensors Actuators, B Chem.*, vol. 290, no. 7, pp. 100–109, 2019.

[8] A. Subasi and M. I. Gursoy, "EEG signal classification using PCA, ICA, LDA and support vector machines," *Expert Syst. Appl.*, vol. 37, no. 12, pp. 8659–8666, 2010.

[9] N. Petrellis, M. Birbas, and F. Gioulekas, "On the design of low-cost IoT sensor node for e-health environment," *Electron.*, vol. 8, no. 2, 2019, Art. no. 178.

[10] W. Kim *et al.*, "Highly reproducible au-decorated ZnO nanorod array on a graphite sensor for classification of human aqueous humors," *ACS Appl. Mater. Interfaces*, vol. 9, no. 7, pp. 5891–5899, 2017.

[11] W. Kim *et al.*, "Paper-based surface-enhanced Raman spectroscopy for diagnosing prenatal diseases in women," *ACS Nano*, vol. 12, no. 7, pp. 7100–7108, 2018.

[12] M.-J. Jeng *et al.*, "Raman spectroscopy analysis for optical diagnosis of oral cancer detection," *J. Clin. Med.*, vol. 8, no. 9, 2019, Art. no. 1313.

[13] A. Purwidyantri *et al.*, "Speckled ZnO nanograss electrochemical sensor for staphylococcus epidermidis detection," *J. Electrochem. Soc.*, vol. 164, no. 6, pp. B205–B211, 2017.

[14] A. K. Gupta *et al.*, "ZnO-Nanorod processed PC-SET as the light-harvesting model for plasmontronic fluorescence Sensor," *Sensors Actuators, B Chem.*, vol. 307, no. 9, 2020, Art. no. 127597.

[15] F. Kayaci, S. Vempati, I. Donmez, N. Biyikli, and T. Uyar, "Role of zinc interstitials and oxygen vacancies of ZnO in photocatalysis: A bottom-up approach to control defect density," *Nanoscale*, vol. 6, no. 17, pp. 10224–10234, 2014.

[16] A. Purwidyantri, C. H. Hsu, C. M. Yang, B. A. Prabowo, Y. C. Tian, and C. S. Lai, "Plasmonic nanomaterial structuring for SERS enhancement," *RSC Adv.*, vol. 9, no. 9, pp. 4982–4992, 2019.

[17] A. Purwidyantri, I. El-Mekki, and C. S. Lai, "Tunable Plasmonic SERS Hotspots on Au-Film over nanosphere by rapid thermal annealing," *IEEE Trans. Nanotechnol.*, vol. 16, no. 4, pp. 551–559, 2017.

[18] S. Szunerits, V. G. Praig, M. Manesse, and R. Boukherroub, "Gold island films on indium tin oxide for localized surface plasmon sensing," *Nanotechnology*, vol. 19, no. 19, 2008, Art. no. 195712.

[19] I. T.Jolliffe, J. Cadima, and J. Cadima, "Principal component analysis: A review and recent developments subject areas," *Phil. Trans. R. Soc. A*, vol. 374, no. 2065, 2016, Art. no. 20150202.

[20] H. Abdi and L. J. Williams, "Principal component analysis," *Wiley Interdiscip. Rev. Comput. Stat.*, vol. 2, no. 4, pp. 433–459, 2010.

[21] S. M. Holland, "Principal components analysis (PCA)," in *Proc. Dept. Geol.*, University of Georgia, Athens, GA, 2008, pp. 1–12.

[22] A. Kushwaha and M. Aslam, "Defect controlled water splitting characteristics of gold nanoparticle functionalized ZnO nanowire films," *RSC Adv.*, vol. 4, no. 40, pp. 20955–20963, 2014.

[23] V. Perumal *et al.*, "Thickness dependent nanostructural, morphological, optical and impedometric analyses of zinc oxide-Gold hybrids: Nanoparticle to thin film," *PLoS One*, vol. 10, no. 12, pp. 1–24, 2015.
[24] L. A. Wali, K. K. Hasan, and A. M. Alwan, "Rapid and highly efficient detection of ultra-low concentration of penicillin G by gold nanoparticles/Porous silicon SERS active substrate," *Spectrochim. Acta - Part A Mol. Biomol. Spectrosc.*, vol. 206, pp. 31–36, 2019.
[25] A. A. Jabbar, A. M. Alwan, and A. J. Haider, "Modifying and fine controlling of silver nanoparticle nucleation sites and SERS performance by double silicon etching process," *Plasmonics*, vol. 13, no. 4, pp. 1171–1182, 2018.
[26] L. Liu *et al.*, "Au-ZnO hybrid nanoparticles exhibiting strong charge-transfer-induced SERS for recyclable SERS-active substrates," *Nanoscale*, vol. 7, no. 12, pp. 5147–5151, 2015.
[27] X. Jiang *et al.*, "Recyclable Au-TiO2 nanocomposite SERS-active substrates contributed by synergistic charge-transfer effect," *Phys. Chem. Chem. Phys.*, vol. 19, no. 18, pp. 11212–11219, 2017.
[28] A. M. Alwan, A. A. Yousif, and L. A. Wali, "The growth of the silver nanoparticles on the mesoporous silicon and macroporous silicon: A comparative study," *Indian J. Pure Appl. Phys.*, vol. 55, no. 11, pp. 813–820, 2017.
[29] J. Wang *et al.*, "Oxygen vacancy induced band-gap narrowing and enhanced visible light photocatalytic activity of ZnO," *ACS Appl. Mater. Interfaces*, vol. 4, pp. 4024–4030, 2012.
[30] X. C. Ma, Y. Dai, L. Yu, and B. B. Huang, "Energy transfer in plasmonic photocatalytic composites," *Light Sci. Appl.*, vol. 5, 2016, Art. no. e16017.
[31] S. G. Park *et al.*, "Fabrication of Au-Decorated 3D ZnO nanostructures as recyclable SERS substrates," *IEEE Sens. J.*, vol. 16, no. 10, pp. 3382–3386, 2016.
[32] S. Lee *et al.*, "Diagnosis in a preclinical model of bladder pain syndrome using a Au/Zno nanorod-based sers substrate," *Nanomaterials*, vol. 9, no. 2, pp. 1–9, 2019.
[33] Y. Hong *et al.*, "Label free diagnosis for colorectal cancer through coffee ring assisted surface enhanced Raman spectroscopy on blood serum," *J. Biophotonics*, pp. 1–30, 2020.
[34] B. Nikola *et al.*, "Highly textured seed layers for the growth of vertically oriented ZnO nanorods," *Crystals*, vol. 9, no. 11, pp. 1–13, 2019.